Instabilities of Shercliffe and Stewartson layers in spherical Couette flow

X. Wei
Department of Engineering, University of Cambridge, Cambridge CB2 1PZ, United Kingdom

R. Hollerbach
Department of Applied Mathematics, University of Leeds, Leeds, LS2 9JT, United Kingdom

(Received 7 May 2008; published 28 August 2008)

We explore numerically the flow induced in a spherical shell by differentially rotating the inner and outer spheres. The fluid is also taken to be electrically conducting (in the low magnetic Reynolds number limit), and a magnetic field is imposed parallel to the axis of rotation. If the outer sphere is stationary, the magnetic field induces a Shercliffe layer on the tangent cylinder, the cylinder just touching the inner sphere and parallel to the field. If the magnetic field is absent, but a strong overall rotation is present, Coriolis effects induce a Stewartson layer on the tangent cylinder. The nonaxisymmetric instabilities of both types of layer separately have been studied before; here, we consider the two cases side by side, as well as the mixed case, and investigate how magnetic and rotational effects interact. We find that if the differential rotation and the overall rotation are in the same direction, the overall rotation may have a destabilizing influence, whereas if the differential rotation and the overall rotation are in the opposite direction, the overall rotation always has a stabilizing influence.

DOI: 10.1103/PhysRevE.78.026309 PACS number(s): 47.20.−k, 47.65.−d

I. INTRODUCTION

The study of free shear layers and their instabilities is one of the oldest problems in fluid dynamics, dating back to the pioneering work of Kelvin [1] and Helmholtz [2]. In this work we will consider two types of shear layer, the magnetically induced Shercliffe layer and the rotationally induced Stewartson layer, which can easily be set up in a differentially rotating spherical shell. Previous work has studied each of these layers and its corresponding instabilities in isolation [3,4]. The basic shear layers are similar in many ways, but their instabilities may be very different. Here we compare and contrast the two problems, and then consider the mixed case, when both magnetic and rotational effects are present.

Previous studies on magnetohydrodynamic spherical Couette flow have included analytic [5–7], numerical [8–10], and experimental [11,12] work, with a variety of imposed magnetic fields. Nonmagnetic Stewartson layers have also been widely studied, in both cylindrical [13–17] and spherical [18–20] geometries.

II. EQUATIONS

We start with two concentric spheres, of radii r_i and r_o, rotating about a common axis (z axis) with angular velocities Ω_i and Ω_o. The fluid filling the shell is taken to be electrically conducting, and a magnetic field $\mathbf{B}=B_0\hat{\mathbf{e}}_z$ is externally imposed. The question then is, what sort of flow states will result as the parameters B_0, Ω_i, and Ω_o are varied, and can the solutions be classified in some systematic way, for example, according to whether they are magnetically or rotationally dominated?

In the reference frame rotating with the outer sphere, the governing equations are

$$\frac{\partial \mathbf{U}}{\partial t} + \mathrm{Re}\,\mathbf{U}\cdot\boldsymbol{\nabla}\mathbf{U} + \mathrm{Ta}\hat{\mathbf{e}}_z\times\mathbf{U} = -\boldsymbol{\nabla}p + \nabla^2\mathbf{U} + \mathrm{Ha}^2(\boldsymbol{\nabla}\times\mathbf{b})\times\hat{\mathbf{e}}_z, \tag{1}$$

$$\nabla^2\mathbf{b} = -\boldsymbol{\nabla}\times(\mathbf{U}\times\hat{\mathbf{e}}_z), \tag{2}$$

where the Hartmann number

$$\mathrm{Ha} = \frac{B_0 r_i}{\sqrt{\mu\rho\nu\eta}} \tag{3}$$

measures the strength of the imposed magnetic field, the Taylor number

$$\mathrm{Ta} = \frac{2\Omega_o r_i^2}{\nu} \tag{4}$$

measures the overall rotation of the whole system, and the Reynolds number

$$\mathrm{Re} = \frac{(\Omega_i-\Omega_o)r_i^2}{\nu} \tag{5}$$

measures the differential rotation of the inner sphere. The density ρ, viscosity ν, diffusivity η, and permeability μ are (constant) material properties of the fluid.

In these equations, length has been scaled by r_i, time by r_i^2/ν, and $\mathbf{U}$ by $(\Omega_i-\Omega_o)r_i$. Finally, the induced magnetic field $\mathbf{b}$ has been scaled by $\mathrm{Rm}\,B_0$, where $\mathrm{Rm}=(\Omega_i-\Omega_o)r_i^2/\eta$ is the magnetic Reynolds number, and Eqs. (1) and (2) have been formulated in the $\mathrm{Rm}\to 0$ limit, in which Rm no longer appears in the equations at all, but only in the interpretation associated with $\mathbf{b}$. See also [3]; the problem considered here is precisely the extension of [3] to include the overall rotation given by Ta.

The boundary conditions associated with (1) are the usual spherical Couette flow conditions

$$\mathbf{U} = r\sin\theta\,\hat{\mathbf{e}}_\phi \quad \text{at } r=r_i, \qquad \mathbf{U}=\mathbf{0} \quad \text{at } r=r_o, \tag{6}$$

where the radii will be fixed at $r_i=1$ and $r_o=3$. For the boundary conditions associated with (2) we take the exterior regions $r<r_i$ and $r>r_o$ to be insulating. As shown in [3], taking these regions to be conducting instead can have dra-

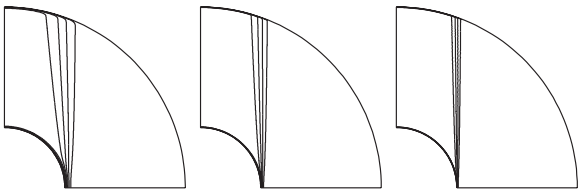

FIG. 1. Examples of the pure Shercliffe layer, showing contours of the angular velocity, with a contour interval of 1/9. From left to right, $\mathrm{Ha}^2=10^4,10^5,10^6$ and $\mathrm{Ta}=\mathrm{Re}=0$ for all three.

matic consequences, yielding a counterrotating jet rather than a shear layer. However, precisely because we want to focus on shear layers here, we consider only the insulating case.

These equations and associated boundary conditions are solved numerically using the spherical harmonics code [21]. We begin by considering the axisymmetric basic states; then, we linearize about these solutions and compute the linear onset of nonaxisymmetric instabilities. Resolutions as high as 300 Legendre functions in θ and 180 Chebyshev polynomials in r were used, and results were tested to ensure that all aspects of the solutions were fully resolved.

III. TWO PURE CASES

A. Basic states

Figure 1 shows the solutions at $\mathrm{Re}=\mathrm{Ta}=0$ and $\mathrm{Ha}^2=10^4,10^5,10^6$, corresponding to an infinitesimal differential rotation, no overall rotation, and an increasingly strong magnetic field. We see the emergence of an increasingly thin shear layer, the Shercliffe layer, located on the so-called tangent cylinder $\mathcal{C}$, the cylinder just touching the inner sphere and parallel to the magnetic field. The origin of this layer is easy to understand in terms of the magnetic tension along the field lines. Fluid columns outside $\mathcal{C}$ are coupled at both end points to the outer boundary only, so they remain at rest. In contrast, fluid columns inside $\mathcal{C}$ are coupled to both boundaries, which are rotating at different angular velocities, 0 at the outer boundary and 1 at the inner boundary, as imposed by (6). These columns then rotate at a rate intermediate between 0 and 1. The result is a jump in angular velocity across $\mathcal{C}$, which is precisely the Shercliffe layer observed in Fig. 1. (Inside $\mathcal{C}$ there are also Hartmann layers at the outer and inner boundaries, accommodating the jump from $\sim 1/2$ in the interior to 0 and 1 at the boundaries. We will not be interested in these boundary layers though.)

Figure 2 shows the solutions at $\mathrm{Re}=\mathrm{Ha}=0$ and $\mathrm{Ta}=10^{3.5},10^4,10^{4.5}$. We again see the emergence of an increasingly thin shear layer, the Stewartson layer, on the same tangent cylinder $\mathcal{C}$ as before. The origin of this layer is also very similar to that of the Shercliffe layer, the only difference being that now it is the Taylor-Proudman theorem that couples fluid columns along the z axis, and not magnetic tension, which is of course entirely absent for $\mathrm{Ha}=0$.

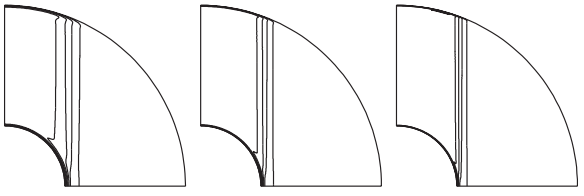

FIG. 2. Examples of the pure Stewartson layer, showing contours of the angular velocity, with a contour interval of 1/9. From left to right, $\mathrm{Ta}=10^{3.5},10^4,10^{4.5}$ and $\mathrm{Ha}=\mathrm{Re}=0$ for all three.

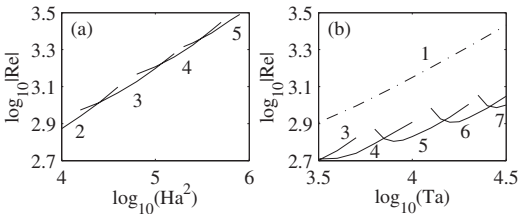

FIG. 3. (a) shows $\log_{10}|\mathrm{Re}_c|$ as a function of $\log_{10}(\mathrm{Ha}^2)$ for the pure Shercliffe layer; (b) shows $\log_{10}|\mathrm{Re}_c|$ as a function of $\log_{10}(\mathrm{Ta})$ for the pure Stewartson layer. The numbers beside individual curves indicate the azimuthal wave numbers m, showing only the most unstable modes. In (b), the solid curves $m=3$ to 7 are for $\mathrm{Re}>0$, whereas the dashed curve $m=1$ is for $\mathrm{Re}<0$.

Despite their similarities, there are also important differences between Shercliffe and Stewartson layers. Note, for example, how the contour lines in the Stewartson layer are almost perfectly parallel, whereas in the Shercliffe layer they spread out somewhat away from the inner sphere. Related to this is the fact that the asymptotics of these two shear layers are also slightly different; the Shercliffe layer consists of a single layer of thickness $\mathrm{Ha}^{-1/2}$ [22], whereas the Stewartson layer consists of a primary layer of thickness $\mathrm{Ta}^{-1/4}$ across which the shear is resolved, but also contains secondary layers of thicknesses $\mathrm{Ta}^{-2/7}$ just inside $\mathcal{C}$ and $\mathrm{Ta}^{-1/3}$ just outside $\mathcal{C}$ [18].

B. Onset of instabilities

The results in Figs. 1 and 2 are all for the case of infinitesimally small differential rotation, $\mathrm{Re}=0$. Now suppose the differential rotation is gradually increased. As the shear across the layers is increased, one might expect the layers to become unstable eventually, to something like a Kelvin-Helmholtz instability. That is, one might expect the initially circular, axisymmetric basic state to adopt a wavy, nonaxisymmetric structure.

The instabilities of the pure Shercliffe layer were considered by [3]; the left panel in Fig. 3 shows their results (Fig. 4a in [3]), over the range of Hartmann numbers shown in Fig. 1. The instabilities of the pure Stewartson layer were considered by [4]; the right panel in Fig. 3 shows these results (Fig. 4 in [4]), again over the range of Taylor numbers shown in Fig. 2. [Note though that the equations here are scaled differently from those in [4] to allow for the possibility of $\mathrm{Ta}=0$ here. The Ekman and Rossby numbers in [4] are related to the Taylor and Reynolds numbers used here by $E=1/(2\mathrm{Ta})$ and $\mathrm{Ro}=2\mathrm{Re}/\mathrm{Ta}$.]

Comparing the two panels in Fig. 3, there are clearly similarities between the two cases. Most obviously, for comparable thicknesses of the underlying shear layers (as indicated in Figs. 1 and 2) the critical Reynolds numbers for the onset

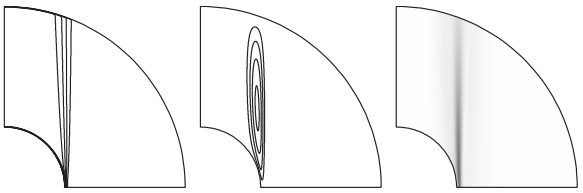

FIG. 4. The Shercliffe layer at $\mathrm{Ha}^2=10^5$, $\mathrm{Re}_c=\pm 1588$, and $\mathrm{Ta}=0$. The left panel shows the angular velocity, with a contour interval of 1/9; the middle panel shows the meridional circulation, with a contour interval of 10^{-4}; the right panel shows the azimuthally integrated kinetic energy of the instability, having wave number $m=3$, as indicated in the left panel of Fig. 3.

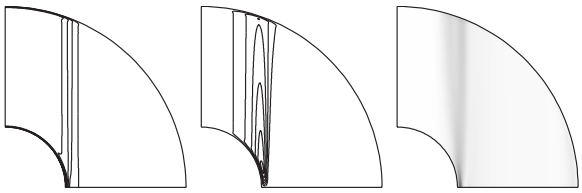

FIG. 5. The Stewartson layer at $\mathrm{Ta}=10^4$, $\mathrm{Re}_c=665$, and $\mathrm{Ha}=0$. The left panel shows the angular velocity, with a contour interval of 1/9; the middle panel shows the meridional circulation, with a contour interval of 10^{-3}; the right panel shows the azimuthally integrated kinetic energy of the instability, having wave number $m=5$, as indicated in the right panel of Fig. 3.

of instabilities are also comparable, with $|\mathrm{Re}_c|\sim 10^3$ for the Ha and Ta ranges shown. Beyond that, in both cases the critical Reynolds numbers increase as the thickness of the shear layers decreases.

However, there is also one crucial difference between the instabilities of these two types of shear layer, more fundamental than any difference between the shear layers themselves. Specifically, for the pure Shercliffe layer, the results are invariant to the sign of Re—that is, the direction in which the inner sphere rotates. The easiest way to see this is to note that reversing the rotation of the inner sphere is equivalent to turning the entire system upside down. This merely reverses the sign of the imposed magnetic field though, which clearly has no effect.

In sharp contrast, the results for the Stewartson layer are not invariant to the sign of Re. One can, of course, still imagine turning the system upside down, but instead of reversing the magnetic field, this now reverses the sense of the overall rotation. And unlike the magnetic field, whose sign does not matter, the sign of the overall rotation does matter. That is, instead of reversing the sign of Re one could just as well reverse the sign of Ta, but the result is still not equivalent to the original configuration. Having Re and Ta of the same sign is fundamentally different from having them of the opposite sign.

Returning to the right panel in Fig. 3 then, we note that $\mathrm{Re}>0$ and $\mathrm{Re}<0$ do indeed yield strikingly different instabilities. Positive Re has increasingly large azimuthal wave numbers m for increasingly large Ta, exactly as one would expect for a Kelvin-Helmholtz-type instability, whereas negative Re has $m=1$ over the entire range of Ta shown here. Comparing with the $\pm$Re invariant Shercliffe results in the left panel, we see that these are more like the $\mathrm{Re}>0$ Stewartson results, in that they also show a progression to higher m.

One reason for considering the mixed Shercliffe-Stewartson problem then is simply to see how this $\pm$Re asymmetry manifests itself in this case and at what point the results are more like the symmetric Shercliffe problem or more like the asymmetric Stewartson problem.

C. Location of the instabilities

First though we consider a few more aspects of the two pure problems: namely, the spatial location of the instabilities. Figure 4 shows the Shercliffe case, Fig. 5 the $\mathrm{Re}>0$ Stewartson case. The first panels in each figure show the angular velocity, as before in Figs. 1 and 2. One point to note here is how similar these solutions at nonzero Re are to the $\mathrm{Re}=0$ solutions in Figs. 1 and 2. The inertial term $\mathrm{Re}\mathbf{U}\cdot\boldsymbol{\nabla}\mathbf{U}$ is crucially important in driving the instabilities, but in the basic states themselves it is almost completely balanced by the pressure-gradient term. The second panels show the associated meridional circulation. This is very weak though in comparison with the shear layers and does not appear to play an important role in the instabilities. Finally, the gray shading in the third panels shows the azimuthally integrated kinetic energy of the instabilities—that is, the quantity $\int|\mathbf{u}|^2 r\sin\theta\, d\phi$. As expected, both instabilities are concentrated on the tangent cylinder $\mathcal{C}$, although it is interesting to note that the concentration is far greater in the Shercliffe case than in the Stewartson case.

Figure 6 shows the corresponding results for the $\mathrm{Re}<0$ Stewartson case, the anomalous $m=1$ mode. The instability now appears to have curious gaps in cylindrical radius, resulting in a striped appearance. Furthermore, the instability reaches its maximum concentration not on $\mathcal{C}$, but instead just inside, where the Stewartson layer intersects the Ekman layer on the inner sphere. This would suggest that this anomalous mode is perhaps not a Stewartson layer instability at all, but instead an Ekman layer instability, for which it is well known that the $\mathrm{Re}>0$ case (von Kármán flow) and the $\mathrm{Re}<0$ case (Bödewadt flow) are indeed very different [23].

The numerical tests conducted by [4] considered exactly this possibility and suggest that however plausible this idea may be, it is incorrect: this $\mathrm{Re}<0$ mode is not a Bödewadt instability, but a Stewartson layer instability, just like the $\mathrm{Re}>0$ modes. However, these numerical tests [4], in which the meridional circulation and the Ekman layers were simply deleted from the basic state before computing the instabilities, can be—and indeed have been—criticized as being unphysical, not corresponding to anything that one could actually set up in a laboratory, for example.

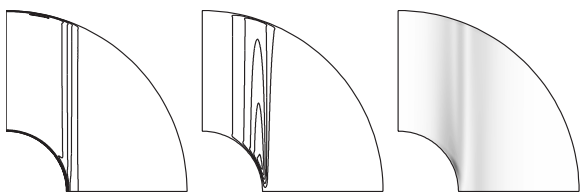

FIG. 6. As in Fig. 5, but with $\mathrm{Re}_c=-1404$ and $m=1$.

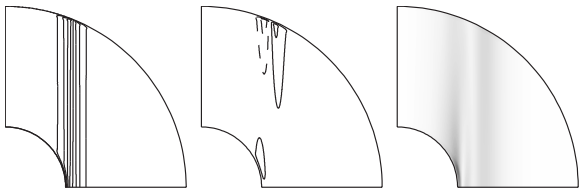

FIG. 7. As in Fig. 6, but with the split outer sphere boundary condition. $\mathrm{Re}_c=-826$ and $m=1$.

We would therefore like to repeat something like this deletion of the meridional circulation and the Ekman layers, but in a way that is physical and could be set up in an experiment. Fortunately, this can be accomplished rather easily: we simply replace the outer boundary condition $\mathbf{U}=\mathbf{0}$ by $\mathbf{U}=r\sin\theta\,\Omega(\theta)\hat{\mathbf{e}}_\phi$ at $r=r_o$, where $\Omega(\theta)$ is 1 inside $\mathcal{C}$ and 0 outside (for numerical reasons the transition is actually smoothed out over a degree or so). Physically this would correspond to having the outer sphere split into differentially rotating segments, with the regions inside the tangent cylinder now corotating with the inner sphere, which is precisely how many Stewartson layer experiments are indeed done [16,20].

Figure 7 shows these results. If we begin by comparing the basic states in Figs. 6 and 7, we see that this new boundary condition has roughly doubled the jump in angular velocity across the shear, because everything inside $\mathcal{C}$ is now corotating with the inner sphere, whereas before the fluid inside $\mathcal{C}$ was rotating at a rate intermediate between 1 at the inner boundary and 0 at the outer. Turning next to the Ekman layers, these have been largely eliminated; if everything inside $\mathcal{C}$ is corotating, there is simply no need for Ekman layers at the boundaries. And correspondingly, the meridional circulation, which is driven by Ekman pumping in the boundary layers, is also dramatically reduced.

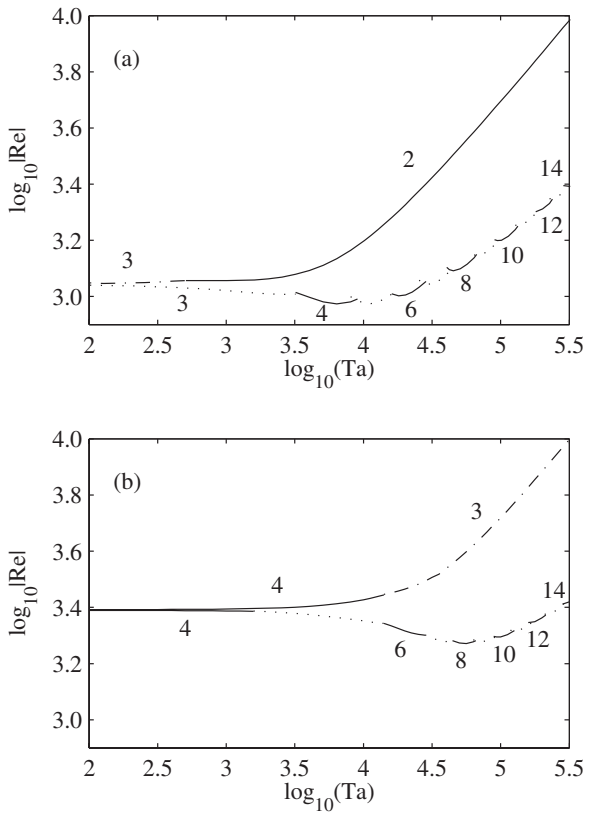

FIG. 8. The critical Reynolds numbers for the onset of instabilities, as functions of $\log_{10}(\mathrm{Ta})$, with $\mathrm{Ta}=10^2$ almost the pure Shercliffe regime and $\mathrm{Ta}=10^{5.5}$ almost the pure Stewartson regime. (a) is for $\mathrm{Ha}^2=10^{4.5}$; (b) is for $\mathrm{Ha}^2=10^{5.5}$. Within each panel the upper set of curves, with decreasing wave numbers, is for $\mathrm{Re}<0$; the lower set of curves, with increasing wave numbers, is for $\mathrm{Re}>0$.

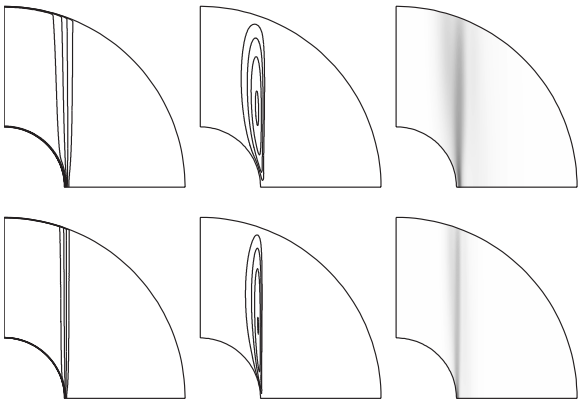

FIG. 9. The top row shows results at $\mathrm{Ha}^2=10^{4.5}$, $\mathrm{Ta}=10^{3.75}$, $\mathrm{Re}_c=946$, and $m=4$, the bottom row at $\mathrm{Ha}^2=10^{5.5}$, $\mathrm{Ta}=10^{4.75}$, $\mathrm{Re}_c=1827$, and $m=8$—that is, at the minima of the $\mathrm{Re}>0$ curves in Fig. 8. The left panels show the angular velocity, with a contour interval of 1/9; the middle panels show the meridional circulation, with a contour interval of 10^{-3} (top) and 5×10^{-4} (bottom); the right panels show the azimuthally integrated kinetic energy of the instabilities.

This new boundary condition has thus accomplished exactly what we wanted, but in a way that is physically realizable, unlike the numerical tests presented in [4]. And if we compare the instabilities in the two cases, then the original boundary condition (Fig. 6) has $m=1$ and $\mathrm{Re}_c=-1404$ and the new boundary condition (Fig. 7) has $m=1$ and $\mathrm{Re}_c=-826$. That is, doubling the shear across the layer roughly halves the critical Reynolds number, exactly as one would expect if it is indeed the shear layer that is triggering the instability. This new boundary condition therefore confirms the claim made by [4] that this anomalous $m=1$ mode is also a Stewartson layer instability (although beyond that there are unfortunately still many aspects of this mode that are not entirely clear).

IV. MIXED CASE

Figure 8 shows stability results for the mixed case, when neither Ha nor Ta is zero. Starting with Hartmann numbers $\mathrm{Ha}^2=10^{4.5}$ and $10^{5.5}$, Ta is increased from 10^2 to $10^{5.5}$ for both positive and negative Re. For $\mathrm{Ta}\ll\mathrm{Ha}^2$, $\pm\mathrm{Re}$ are not surprisingly almost the same. As rotational effects become comparable with magnetic effects, though, the rotationally induced asymmetry becomes more and more pronounced. For positive (negative) Re the wave number increases (decreases), until for $\mathrm{Ta}=10^{5.5}$ we are almost back to the pure

Stewartson regime, with large m for positive Re and small m for negative Re. It is unfortunately not entirely clear why the wave numbers behave in this way, but the fact that there is this smooth transition from the symmetric Shercliffe case to the asymmetric Stewartson cases, for both positive and negative Re, further reinforces the view that even these "anomalous" $m=1$ modes above are not so anomalous after all, but are merely the limiting case in this family of shear layer instabilities.

One other interesting and completely unexpected result in Fig. 8 is this initial decrease in the $\mathrm{Re}>0$ curves, reaching a minimum when $\mathrm{Ta}/\mathrm{Ha}^2 \sim 10^{-0.75} \approx 0.2$. $\mathrm{Ta}/\mathrm{Ha}^2 = O(1)$ is, of course, precisely the regime where rotational and magnetic effects are comparable, so it is not surprising that any interaction between the two would manifest itself most strongly there. That rotational and magnetic effects can destabilize one another even though each separately has a stabilizing influence is also familiar in other contexts, such as Rayleigh-Bénard convection [24]. It is not clear though why this mutual destabilization in this case does not occur for $\mathrm{Re}<0$ as well.

Finally, we wish to consider the spatial structures of both the basic states and the instabilities in this case $\mathrm{Ta}/\mathrm{Ha}^2 = 10^{-0.75}$, where rotational and magnetic effects are interacting most strongly, and see whether they are more like the pure Shercliffe case or more like the pure Stewartson case. Figure 9 shows the results for $\mathrm{Re}>0$; comparing with Figs. 4 and 5, we see that they look more like the pure Shercliffe case. Figure 10 shows the results for $\mathrm{Re}<0$; comparing with Figs. 4 and 6, we see that the basic state again looks more like the pure Shercliffe case. The instabilities though have aspects in common with both the Stewartson case (namely, this striped appearance), as well as the Shercliffe case (namely, the concentration more outside $\mathcal{C}$), rather than in the equatorial region as in the Stewartson case.

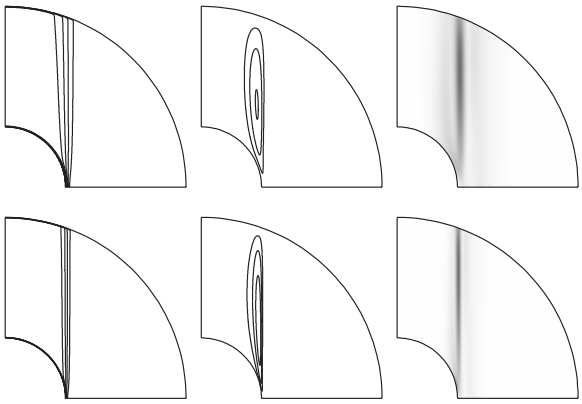

FIG. 10. As in Fig. 9, but for $\mathrm{Re}<0$, with $\mathrm{Ha}^2=10^{4.5}$, $\mathrm{Ta}=10^{3.75}$, $\mathrm{Re}_c=-1324$, and $m=2$ for the top row and $\mathrm{Ha}^2=10^{5.5}$, $\mathrm{Ta}=10^{4.75}$, $\mathrm{Re}_c=-3661$, and $m=3$ for the bottom row.

V. CONCLUSION

In this work we have explored the stability of two types of free shear layers that may be set up by magnetic and rotational effects. Although the shear layers themselves are very similar for the two effects, the instabilities are quite different in one important aspect—namely, that in the magnetic Shercliffe case they are invariant to the sign of the differential rotation that induces them, whereas in the rotational Stewartson case they are not. However, as different as the $\pm$Re pure Stewartson cases may at first sight appear to be, by considering the mixed case, we showed that there is in fact a smooth progression from the invariant Shercliffe limit to both of the $\pm$Re Stewartson cases, suggesting that these cases are not so different after all.

[1] Lord Kelvin, Philos. Mag. **42**, 362 (1871).
[2] H. von Helmholtz, Philos. Mag. **36**, 337 (1868).
[3] R. Hollerbach and S. Skinner, Proc. R. Soc. London, Ser. A **457**, 785 (2001).
[4] R. Hollerbach, J. Fluid Mech. **492**, 289 (2003).
[5] S. V. Starchenko, Phys. Fluids **10**, 2412 (1998).
[6] N. Kleeorin, I. Rogachevskii, A. Ruzmaikin, A. Soward, and S. Starchenko, J. Fluid Mech. **344**, 213 (1997).
[7] E. Dormy, D. Jault, and A. M. Soward, J. Fluid Mech. **452**, 263 (2002).
[8] R. Hollerbach, Proc. R. Soc. London, Ser. A **444**, 333 (1994).
[9] E. Dormy, P. Cardin, and D. Jault, Earth Planet. Sci. Lett. **160**, 15 (1998).
[10] R. Hollerbach, E. Canet, and A. Fournier, Eur. J. Mech. B/Fluids **26**, 729 (2007).
[11] D. R. Sisan, N. Mujica, W. A. Tillotson, Y. M. Huang, W. Dorland, A. B. Hassam, T. M. Antonsen, and D. P. Lathrop, Phys. Rev. Lett. **93**, 114502 (2004).
[12] H.-C. Nataf, T. Alboussiere, D. Brito, P. Cardin, N. Gagniere, D. Jault, J.-P. Masson, and D. Schmitt, Geophys. Astrophys. Fluid Dyn. **100**, 281 (2006).
[13] K. Stewartson, J. Fluid Mech. **3**, 17 (1957).
[14] R. Hide and C. W. Titman, J. Fluid Mech. **29**, 39 (1967).
[15] F. H. Busse, J. Fluid Mech. **33**, 577 (1968).
[16] W. G. Früh and P. L. Read, J. Fluid Mech. **383**, 143 (1999).
[17] A. Aguiar and P. Read, Meteorol. Z. **15**, 417 (2006).
[18] K. Stewartson, J. Fluid Mech. **26**, 131 (1966).
[19] R. Hollerbach, B. Futterer, T. More, and C. Egbers, Theor. Comput. Fluid Dyn. **18**, 197 (2004).
[20] N. Schaeffer and P. Cardin, Phys. Fluids **17**, 104111 (2005).
[21] R. Hollerbach, Int. J. Numer. Methods Fluids **32**, 773 (2000).
[22] P. H. Roberts, Proc. R. Soc. London, Ser. A **300**, 94 (1967).
[23] H. A. Jasmine and J. S. B. Gajjar, Philos. Trans. R. Soc. London, Ser. A **363**, 1131 (2005).
[24] S. Chandrasekhar, *Hydrodynamic and Hydromagnetic Stability* (Clarendon, Oxford, 1961).